Journal of Power Sources 196 (2011) 9767–9773

Contents lists available at ScienceDirect

Journal of Power Sources

journal homepage: www.elsevier.com/locate/jpowsour

Solid polymer electrolytes with sulfur based ionic liquid for lithium batteries

Aaron S. Fisher[a], Mian B. Khalid[b], Matthew Widstrom[c], Peter Kofinas[b,*]

[a] Department of Chemical and Biomolecular Engineering, University of Maryland, College Park, MD 20742, United States
[b] Fischell Department of Bioengineering, University of Maryland, College Park, MD 20742, United States
[c] Department of Materials Science and Engineering, University of Maryland, College Park, MD 20742, United States

ARTICLE INFO

Article history:
Received 20 June 2011
Received in revised form 25 July 2011
Accepted 26 July 2011
Available online 4 August 2011

Keywords:
Lithium battery
Triethylsulfonium bis(trifluorosulonyl) imide
Polymer electrolytes
Ionic liquids

ABSTRACT

The electrochemical properties of a solid hybrid polymer electrolyte for lithium batteries based upon tri-ethyl sulfonium bis(trifluorosulfonyl) imide (S_2TFSI), lithium TFSI, and poly(ethylene oxide) (PEO) is presented. We have synthesized homogenous freestanding films that possess low temperature ionic conductivity and wide electrochemical stability. The hybrid electrolyte has demonstrated ionic conductivity of 0.117 mS cm^{-1} at 0 °C, and 1.20 mS cm^{-1} at 25 °C. At slightly elevated temperature ionic conductivity is on the order of 10 mS cm^{-1}. The hybrid electrolyte has demonstrated reversible stability against metallic lithium at the anodic interface and >4.5 V vs. Li/Li$^+$ at the cathodic interface.

1. Introduction

Battery technology has been unable to become more powerful, while still remaining safe to the end consumer. To accomplish this a new generation of electrolytes will need to be developed that replaces organic carbonate based electrolytes [1]. Solid polymer electrolytes are an alternative to liquid combustible systems because they possess superior voltage, temperature and mechanical stability. These benefits though come with a large trade off with conductivity [1–5]. Poly(ethylene oxide) (PEO) has conductivity problems at ambient temperatures because of its semi-crystalline nature. Thus, it has become a research focus to energetically favor the amorphous phase by inclusion of a secondary block copolymer [6], lower molecular weight polymers [7], ceramic particles [8,9], carbonate solvents [10] or ionic liquids (ILs) [11–13]. ILs are attractive additives because they are tunable systems that possess wide temperature and voltage stability while having appreciable conductivity without compromising safety.

ILs are considered tunable solvents, as the anion and cation can be chosen to control the macro-properties of the electrolyte. Of the most commonly used IL architectures, the imidazolium architecture [14] has the highest conductivity and thus makes it an ideal starting point for the development of an electrolyte. However, this same scaffold has encountered problems with its stability at low voltages and its intercalation into the graphite anode resulting in exfoliation and rapid capacity fade [15,16]. Pyrrolidinium architectures [17] have been investigated because they possess high native ionic conductivity values. However, because they are poor solvents of lithium they demonstrate limited lithium conductivity values. By combining the polymer electrolyte with ILs, a hybrid system can be constructed that will meet the performance standards for a battery electrolyte while still maintaining adequate mechanical properties as a solid [18].

Shin et al. [11] have shown that adding 1-butyl-1-methyl pyrrolidinium TFSI to PEO results in a marked increase in ionic conductivity between 1 and 2 orders of magnitude. However the upper limit of conductivity achievable in the polymer electrolyte is still one order less than the conductivity of the neat ionic liquid. Additionally the large ratio of ionic liquid to polymer in Shin's optimized electrolyte has adverse effects upon the transference number, inherently limiting the capacity that can be delivered by lithium with each cycle [19,20]. This led to interest in novel IL scaffolds that would overcome these observed limitations while mimicking the preferred method of Li$^+$ conduction through the polymer chains [21,22]. Research into sulfur and phosphorous based systems has demonstrated superior electrochemical stability and conductivity values relative to nitrogen based architectures [23,24].

Electrolyte research involving ILs has been largely limited to nitrogen based architectures. However, sulfur based architectures promise to provide superior electrical properties, which ultimately will allow these hybrid polymer ionic liquid electrolytes to become the next generation of solid electrolytes. The current polymer-ionic liquid systems are limited by problems with the ionic liquid, and it

* Corresponding author. Tel.: +1 301 405 7335; fax: +1 301 3146868.
E-mail address: kofinas@umd.edu (P. Kofinas).

0378-7753/$ – see front matter © 2011 Elsevier B.V. All rights reserved.
doi:10.1016/j.jpowsour.2011.07.081

is hoped that the incorporation of novel ionic liquids chemistries, based on sulfur, will permit innovation beyond the current systems. Our research has focused on the development of hybrid electrolyte structures that blend sulfur based cations with PEO for improved performance as electrolytes in lithium batteries. We report on the mechanical and electrochemical characterization of this system.

2. Experimental

2.1. Materials

LiTFSI ($LiN(SO_2CF_3)_2$), and lithium, aluminum and platinum foil were purchased from Aldrich and used as received. Poly(ethylene oxide) (Mw 300k) and triethyl sulfide iodide were purchased from Alfa Aesar and used as received.

2.2. RTIL preparation

S_2TFSI ($S(CH_2CH_3)_3$ TFSI) was synthesized according to previous literature [25]. Briefly, S_2I was stirred with LiTFSI (10% stoichiometric excess) in DI H_2O for 4 h. The IL was then diluted with dichloromethane and washed 5× with water until no precipitate formed by $AgNO_3$. The organic layer was then dried under high vacuum at 60 °C for 24 h. Characterization was performed by NMR on a Bruker AV-400 high resolution NMR. ^{1}H, ^{13}C and ^{19}F (TFA capillary reference) were performed in deuterated methanol. Mass spectroscopy measurements were performed on a JEOL AccuTOF-CS ESI-TOF mass spectrometer. ESI^+/ESI^- modes were looked at over the m/z range of 80–500. ^{1}H: 3.3341 (q, J = 7.4 Hz, 6 H), 1.4694 (t, J = 7.4 Hz, 9 H), ^{13}C: 120.213, 32.681, 7.961, ^{19}F: 41.41. ESI^+: 119.03285, ESI^-: 279.92384.

2.3. Electrolyte preparation

The electrolyte films of different composition were solution cast from tetrahydrofuran onto Bytac molds in an MBRAUN Labmaster 100 argon glove box. The resultant films were dried for several days at 50 °C, before being placed into CR2032 coin cell enclosures for electrolyte testing. All constructed cells are annealed for 3 h at 50 °C prior to any electrochemical testing.

2.4. Electrolyte characterization

Differential scanning calorimetry (DSC) measurements were performed on a TA Instruments Q100 differential scanning calorimeter. Samples were hermetically sealed in Al pans under Ar prior to measurements. Samples were run using a heat/cool/heat method to erase thermal history at a heating rate of 10 °C min^{-1} and a cooling rate of 5 °C min^{-1} from −50 °C to 120 °C.

Conductivity measurements for electrolytes were performed in a SS/electrolyte/SS coin cell set up on a Solartron 1287A/1255B platform over the frequency range 1 MHz to 1 Hz. Testing parameters were controlled by the associated CorrWare and ZPlot software, while data analysis was performed using CorrView, ZView and Origins 8. All temperature testing was done in a RevSci IncuFridge with ±0.5 °C temperature accuracy.

Raman spectroscopy was performed on a Horiba Yvon LabRam ARAMIS using a 100× objective, a 600 gr mm^{-1} grating, a 100 μm hole, a 100 μm slit, a D 0.3 filter and a 633 nm HeNe laser.

Cyclic voltammetry was performed on an Arbin BT2000 to determine the cyclability of the electrolyte. Tested cells were cycled 500 times at room temperature at rate of 5 mV s^{-1}. Pt/electrolyte/Li cells were cycled from 2.5 V to 4.7 V vs. Li/Li$^+$ reference; Al/electrolyte/Li were cycled from 2.5 V to 5.0 V vs. Li/Li$^+$ reference. The half cell potential for Li/Li$^+$, which is used as the reference for all voltammetry measurements, is ∼3.04 V relative to the NHE.

Lithium stripping-plating experiments were performed on the Solartron set-up to determine the interfacial stability and reversibility of the electrolyte material. The electrolyte was sandwiched between two lithium electrodes. A current density of 0.1 mA cm^{-2} was applied to the film and was reversed every hour. 100 cycles, each consisting of 1 h positive current and 1 h negative, were applied to the cell at 45 °C. Impedance spectroscopy was periodically conducted to monitor development of resistance at the interface during the galvanostatic cycling.

3. Results and discussion

Sulfur based ILs were selected because of their high initial conductivity and wide electrochemical stability. Among possible cation scaffolds triethyl sulfonium was chosen for its structural similarity to PEO, as it possess a thioethylene moiety (C–C–S). As a well known lithium ion conductor, PEO with its backbone of repetitive oxyethylene (C–C–O) sequences allows lithium to be coordinated to oxygen units as it moves along the voltage gradient. This association between the polymer backbone and IL is believed to favor lithium as the dominant charge carrier in the electrolyte. Additionally, the IL would plasticize the high molecular weight PEO allowing for increased chain mobility at low temperatures. The anion was selected to allow for elevated temperature applications, and also for the common anion effect with the lithium salt. This led to the widely available TFSI anion, which is only limited because of its instability at high voltages against aluminum. The electrolyte

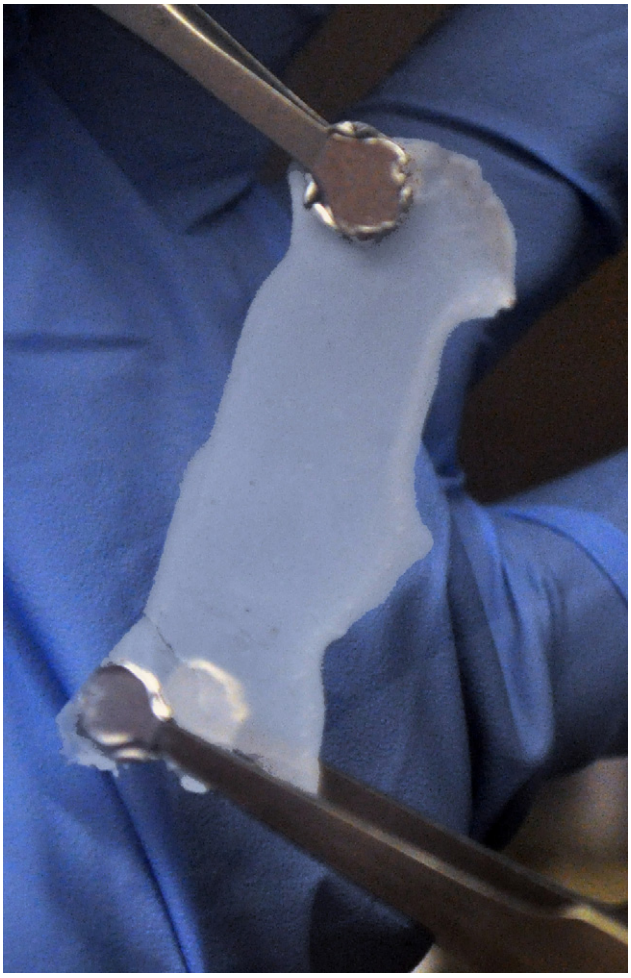

Fig. 1. Picture of thin film solid electrolyte in Ar atmosphere. Electrolyte is ∼5 cm × 2 cm.

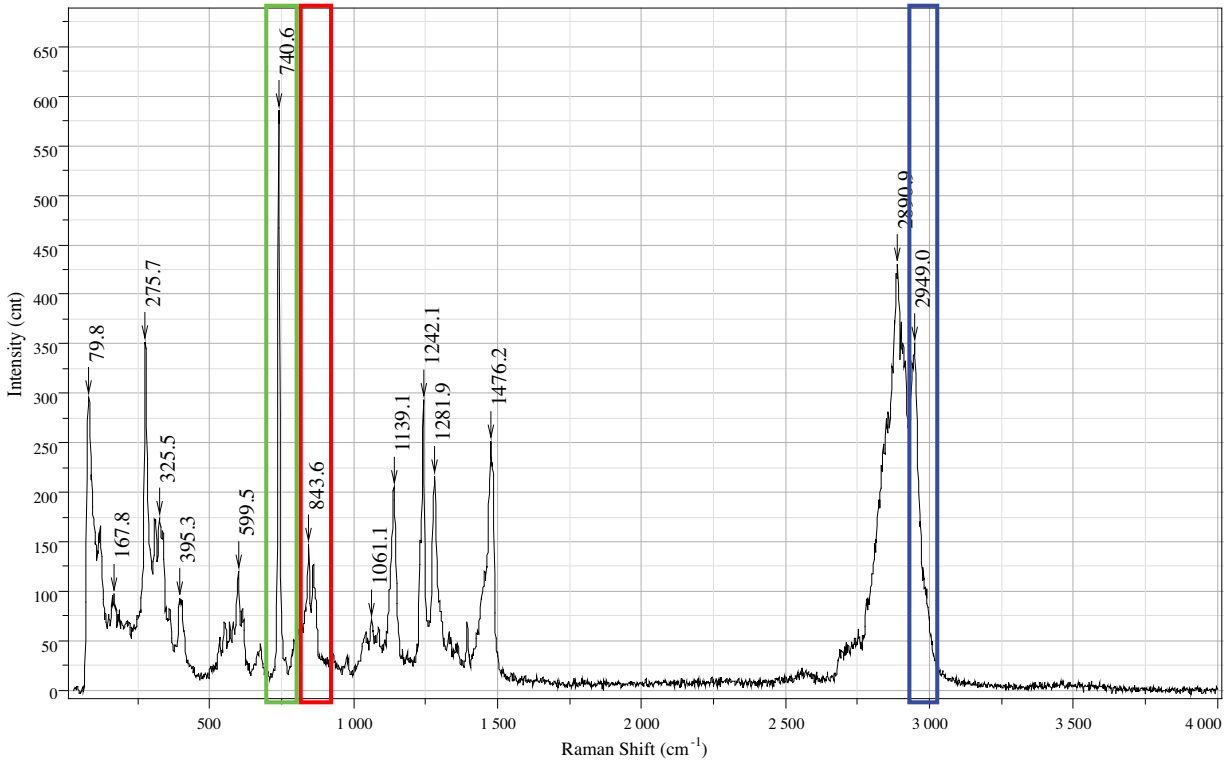

Fig. 2. Raman spectra of IL-1.0 hybrid polymer electrolyte. Indicated areas are as follows: green, LiTFSI 712–769 cm^{-1}; red, PEO 820–886 cm^{-1}; blue, S_2TFSI 2920–2979 cm^{-1}. (For interpretation of the references to color in this figure legend, the reader is referred to the web version of the article.)

is formed by solution casting to create a homogenous film. Four ratios of ionic liquid were evaluated, with constant ratio of polymer to salt to measure the observed properties. The ratio of PEO to lithium salt was selected from a literature survey, leading us to an O/Li^+ of 20:1 [11,26]. The IL ratio was selected to give a broad base without compromising the ability to form thin films. The molar ratios tested were 20 PEO:1 LiTFSI:x S_2TFSI, where x = 0, 0.5, 1.0, and 1.5. Henceforth the electrolytes are referenced by the molar ratio of IL.

After drying, the films formed opaque free standing solid membranes (Fig. 1), which are strong enough to be rolled and manipulated by hand. Raman spectroscopy was performed on the hybrid solid electrolyte to confirm its homogeneity. Each component's spectrum was individually taken before rastering the laser beam over a 50 μm^2. The spectra of IL-1.0 can be seen in Fig. 2 with the relevant integration areas highlighted (Green: LiTFSI 712–769 cm^{-1}, red: PEO 820–886 cm^{-1}, blue: S_2TFSI 2920–2979 cm^{-1}). The color intensity in Fig. 3(a)–(c) corresponds to the integral of the chosen area (darker = greater) with Fig. 3(d) corresponding to the overlay of the three color images. The small changes in the depth of color are believed to be largely the result of the imaging of a dimpled surface, which ultimately affected our ability to focus the beam light in a constant xy-plane over the entire sample. The casting technique results in as-cast films having a variable thickness when observed under a microscope. However, during electrochemical testing this limitation is handled during the annealing process, wherein pressure and temperature are applied to generate uniform contact between the electrode and the electrolyte. Additionally, minor color variations are observed due to the difficulty in selecting peak regions, as there was generally little buffer between peaks of interest and overlapping peaks from other components. The coloring of the overlaid graphs is consistent over the imaged area confirming the homogeneity on the microscale of the electrolyte.

Conductivity is a function of temperature, especially in polymer electrolyte wherein chain mobility is largely responsible for conduction of ions. DSC was performed on the electrolyte to observe any thermal hysteresis over operational temperature. Fig. 4 shows the relevant portion of the cooling and heating cycles of the electrolytes; no peaks were observed outside this region. With increasing concentration of additives, the transition temperatures decrease leading to polymer blends that are amorphous at room temperature. This is preferred because lithium ion conductivity in PEO depends on polymer chain mobility. The large hysteresis can be shown in each of the tested formulations as there is a 20–30 °C difference between the heating and cooling transition temperatures. These differences remained large despite slower heating and cooling rates. The large superheating and cooling effects is believed to be a result of the ionic liquid as this phenomenon is typically seen in the DSC of neat ILs. It is also of note that the IL-1.0 and IL-1.5 formulation are solid at room temperature, despite the thermograms indicating the hybrid electrolyte is in a region between its freezing point and melting point. Lastly with increasing ionic liquid concentration the transition peaks become broader. The trend in the thermograms confirms the increased presence of the amorphous lithium conducting phase at lower temperature. The dry nature of our electrolyte is further confirmed with the absence of water peaks at either 0 or 100 °C.

With this difference between heating and cooling cycles we chose to measure the AC impedance while both heating and cooling our samples. The heating cycles can be seen in Fig. 5(a) of a SS/electrolyte/SS set-up. At 0 °C IL-1.5 has sufficient ionic conductivity (>0.1 mS cm^{-1}) to be useful in battery applications. At room temperature ionic conductivity is on the order of 1 mS cm^{-1}, while at 35 °C the conductivity of the optimum system is 2.95 mS cm^{-1}. This latter temperature is of great interest because it is close to the temperature of the human body, wherein the safety of electrolyte systems limits the deployment of medical devices.

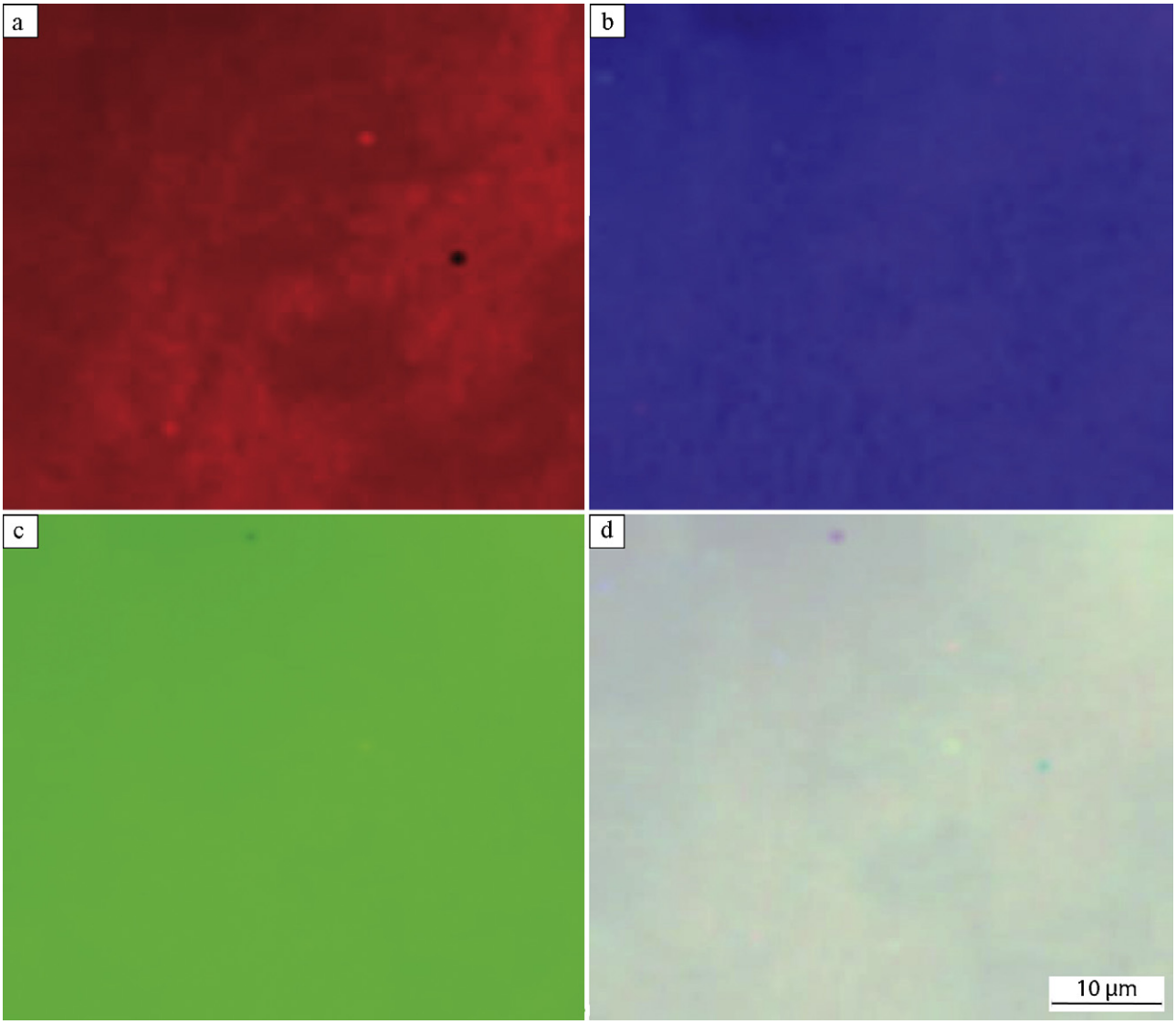

Fig. 3. Confocal Raman spectroscopy of 50 μm^2. Intensity indicates area under the peak. (a) PEO 820–886 cm^{-1}, (b) S_2TFSI 2920–2979 cm^{-1}, (c) LiTFSI 712–769 cm^{-1} and (d) component overlay.

When comparing the conductivity data to each electrolyte's thermogram, a jump in conductivity is observed at the melting temperature, which corresponds to the transition from semicrystalline to melt in the polymer matrix. On either side of this point the conductivity increases linearly over inverse *T*, however, at this temperature the value of this slope changes resulting in smaller increases in conductivity over continued temperature increases.

At low temperatures the addition of IL results in a roughly 3 order of magnitude increase in ionic conductivity, which at higher temperatures diminishes to roughly 1 order of magnitude. This decrease in gain seen by adding IL over increased temperature is believed to be the result of greater reliance on enhanced chain mobility, which leads to greater ionic conductivity in the IL-0 electrolyte. Chain mobility of the PEO systems is largely dependent on the absence of crystalline regions, which occurs above the transition determined from DSC, which is confirmed by the conductivity data. Additionally greater IL concentrations result in diminished increases in conductivity, as seen by the close overlap of IL-1.0 and IL-1.5. This is an agreement with previous hybrid polymer electrolyte systems, whereby the ionic conductivity asymptotically approached that of the pure IL [13].

The observed ionic conductivity values exceeded those of the comparison pyrrolidinium system with significantly less IL. For comparison, the system closest to IL-1.5 ($x = 1.73$), is projected to cross the 0.1 mS cm^{-1} at ~15 °C, a full 15 °C greater than our optimal conductivity system [13]. At slightly elevated temperatures the difference in conductivity between the pyrrolidinium and triethyl sulfonium is diminished, but the sulfur based system still maintains improved conductivity. Given the numerous constraints applied to selecting an electrolyte system [18], the confirmation of our hypothesis that triethyl sulfonium based systems mimic the polymer, bodes well for increased performance by using our hybrid solid polymer electrolyte.

Fig. 5(b) is an isolation of IL-1.5 for the heating and cooling cycles. All data points overlap except for 35 °C, which is markedly different (6.40 mS cm^{-1} (cooling) to 2.95 mS cm^{-1} (heating)). This correlates with the transition temperature determined from DSC (38.40 °C). As expected for the cooling curve which approaches the transition from the melt, the electrolyte is able to supercool until it undergoes a transition prior to the temperature point collected at 25 °C. The heating curve peak occurs at a higher temperature and thus the order of magnitude increase in conductivity associated with the transition is not seen until the 45 °C temperature point.

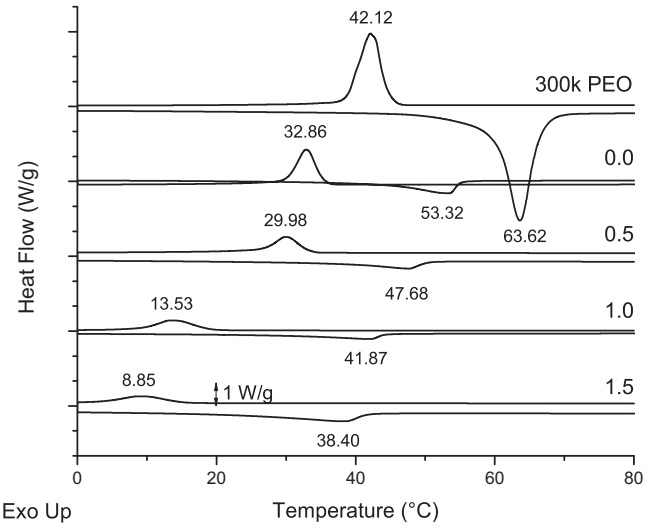

Fig. 4. Selected portion of thermograms from indicated electrolyte mixtures. Heating rate was 10 °C min^{-1} and cooling rate was 5 °C min^{-1} in a heat/cool/heat format with endpoints of −50 °C and 120 °C. Each thermogram is offset 3 W g^{-1}, and each tick mark on the *y*-axis is 1 W g^{-1}. Ratio is moles of 20 PEO:1 LiTFSI:*x* S_2TFSI, where *x* is indicated in the figure.

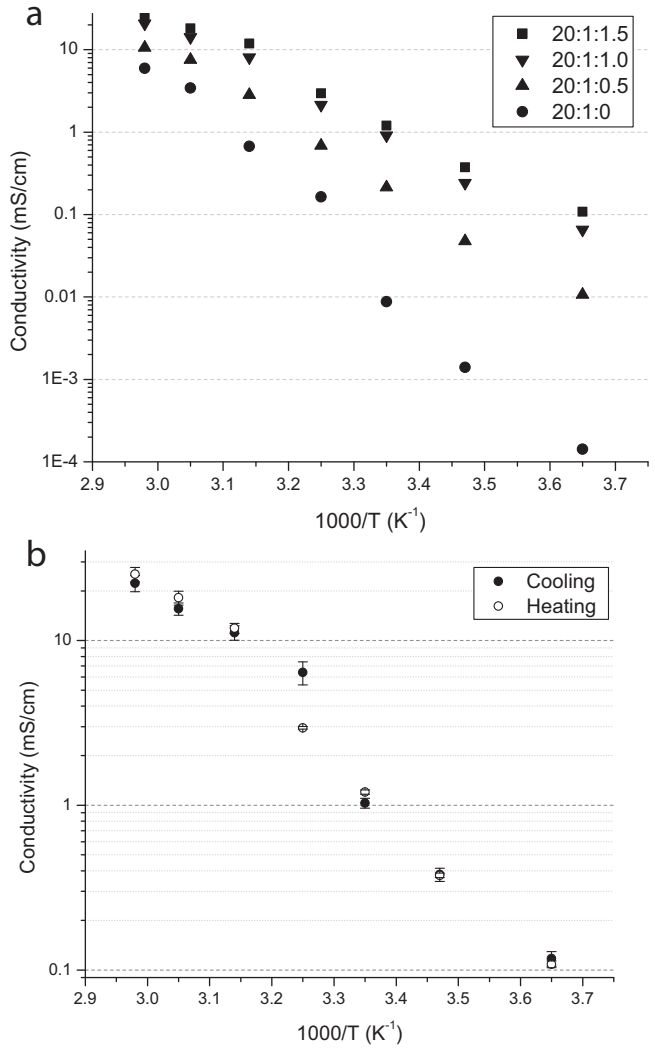

Fig. 5. (a) Conductivity over varied temperature for selected electrolyte over the heating cycle. Ratio is moles of PEO:LiTFSI:S_2TFSI. (b) Effect of thermal history on measured conductivity of IL-1.5 electrolyte.

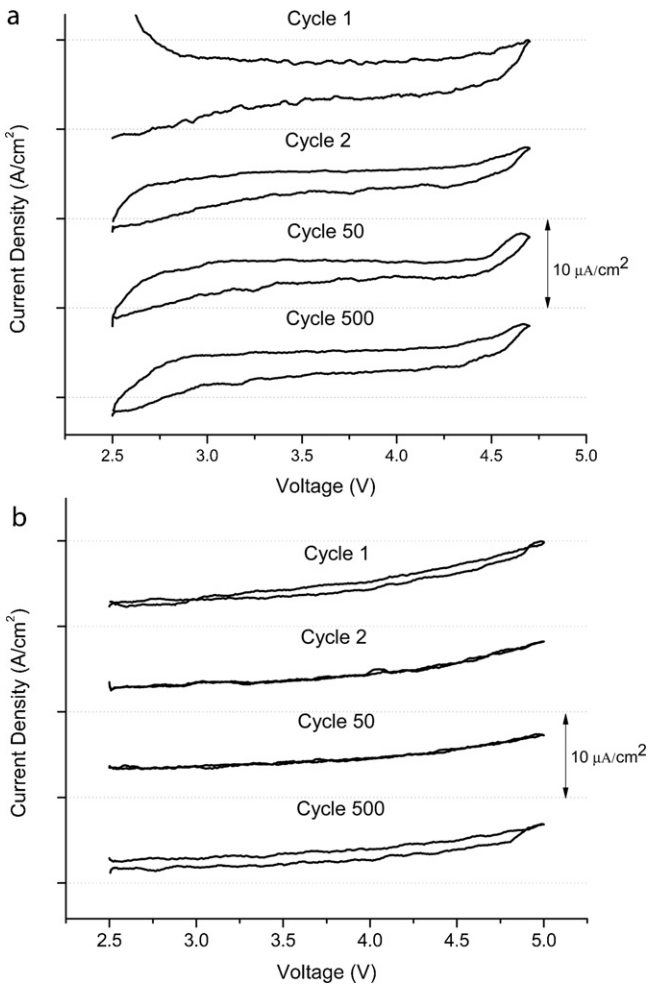

Fig. 6. (a) Cyclic voltammetry of Li/IL-1.0/Pt cell. The voltage was cycled from 2.5 to 4.7 V vs. Li/Li$^+$ at a rate of 5 mV s^{-1} at rt. The current remains relatively constant over the whole voltage range until the upper cathodic limit. Minimal decrease in current is observed from the 1st to 500th cycle. (b) Cyclic voltammetry of a Li/IL-1.0/Al cell. The voltage was cycled from 2.5 to 5.0 V vs. Li/Li$^+$ at a rate of 5 mV s^{-1} at rt.

Considering this, great care was taken to equilibrate cells above room temperature for extended periods of time before cycling.

Electrolytes in lithium batteries, besides being thermally stable lithium ion conductors, need to possess sufficiently wide reversible electrochemical stability against Li/Li$^+$. Stability to the cathode (cathodic stability) should meet or exceed the potential of current carbonate based electrolytes. Stability to the anode (anodic stability) should allow for the utilization of low voltage anodes by formation of a stable solid–electrolyte interphase (SEI).

Reversible cathodic stability in the IL-1.0 electrolyte was attained using cyclic voltammetry of a Li/electrolyte/Pt cell, cycled from 2.5 to 4.7 vs. Li/Li$^+$ for 500 cycles. Platinum was initially used as the counter electrode due to documented concerns in the literature of instability of the TFSI$^-$ anion against Al [27]. In Fig. 6(a) selected cycles show the reversible stability of the electrolyte that exceeds 4.5 V. In cycle 1 there is a clear breakdown near the upper voltage limit, which diminishes in magnitude with further cycling. After the first forward sweep there is a clear decrease in the current density, which is the result of increased resistance. The ability of the hybrid electrolyte to achieve high voltages against lithium is confirmed, ultimately presenting further ability for the development of high power lithium batteries that rely on high voltage cathodes.

In addition to testing our electrolyte system with a Pt counter electrode we decided to investigate its stability against aluminum

Table 1
Resistance and capacitance of equivalent circuit elements from the impedance scans after stated stripping/plating step. The semicircles were modeled as a circuit containing the electrolyte resistance in series to an RC circuit.

Cycle	0	5	10	25	50	75	100
R_e (Ω)	136.61	118.84	112.71	108.65	115.57	124.13	133
R_{ct} (Ω)	1300.6	1445	1576.6	1812.3	2179	2533.7	2822.2
C_{dl} (F)	3.58E-07	3.16E-07	3.08E-07	3.06E-07	3.08E-07	3.07E-07	3.06E-07

in the interest of commercial viability. Aluminum is nearly ubiquitously used as the cathodic current collector and as such its success or failure against this common component needed to be documented. In Fig. 6(b) IL-1.0 is cycled from 2.5 to 5 V against Li/Li$^+$ for 500 cycles. Over the entire cycling process there was minimal current decay indicating stability against high voltage commercial cathodes. The electrolyte as formulated does in fact appear to have promise for 5 V cathode systems. Further electrolyte testing conducted after completion of this test (not pictured) does indicate electrolyte stability that would provide a buffer zone above cathodes with a 5 V discharge potential.

To document the long term stability of the IL-1.0 electrolyte against lithium, galvanostatic cycling was conducted that involves aggressively stripping and plating lithium. A current density of 0.1 mA cm^{-2} was reversed every hour for 100 cycles at 45 °C with intermittent testing of the conductivity via impedance spectroscopy. Selected cycles can be seen in Fig. 7(a), which show that

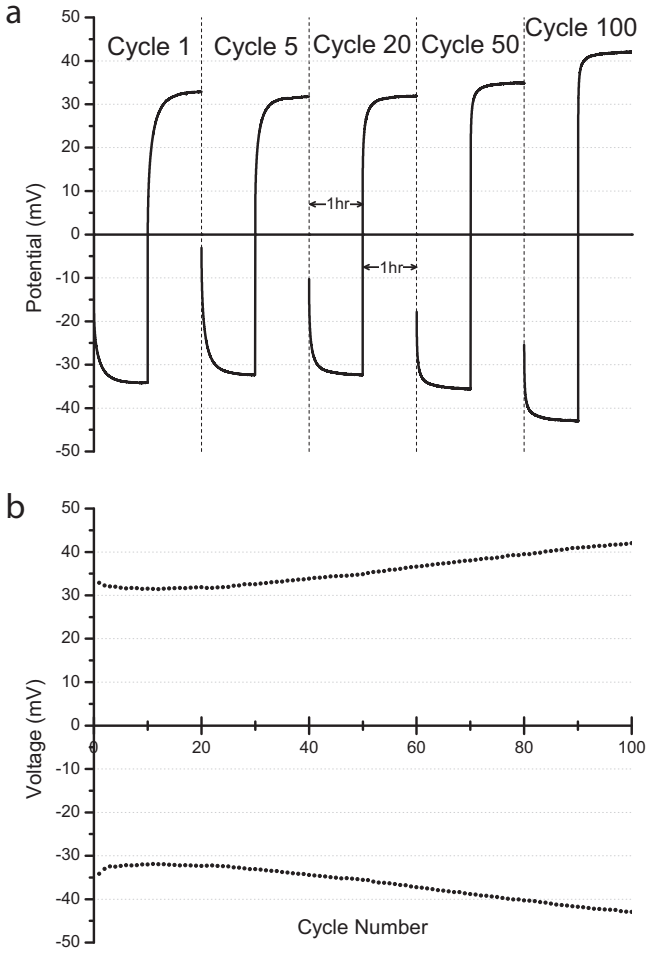

Fig. 7. (a) Measurement of IL-1.0 overpotential as a function of time. Cycle number is as indicated in the legend. (b) Value of overpotential of the electrode–electrolyte interface at the end of each 2 h cycle (1 h charged followed by 1 h discharge both at 0.1 mA cm^{-2}) as a function of cycle number. Testing was conducted at 45 °C.

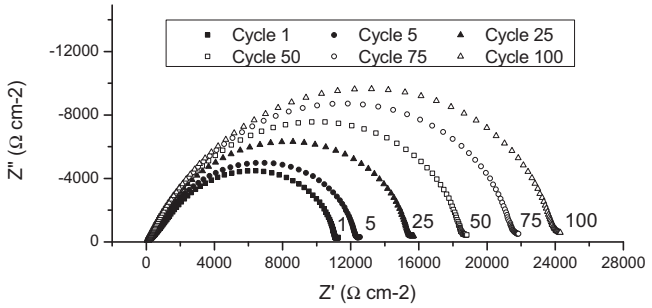

Fig. 8. Nyquist plot of electrolyte during overvoltage study. Frequency range is 1 MHz to 1 Hz.

the electrolyte has a delayed response to the current. Initially the plateau region takes over 30 min to achieve. Over the first 20 cycles this time reduces by half and the cell is able to reach steady state in ~15 min.

The overvoltage at the end of each half-cycle is plotted in Fig. 7(b). There is an initial decrease in the value followed by a constant value for the succeeding 20 cycles. This constant period is then followed by a steady increase in the overvoltage for each successive cycle, until the completion of the test. This steady growth of the resistance in the electrolyte is attributed to the increase in thickness of the SEI layer as determined by impedance spectroscopy. The Coloumbic efficiency of the plating and stripping cycles were evaluated to determine the reversibility of lithium transport. The first cycle has an efficiency of 91.1%, which is believed to be the result of the development of SEI layer. In the 2nd cycle this efficiency quickly jumps to 98.3% and remains close to 98% for the remainder of the 100 cycles.

The selected impedance scans (Fig. 8) show a constantly increasing low frequency intercept of the electrolyte. The Nyquist plots from Fig. 8 were then modeled using an equivalent circuit consisting of the electrolyte resistance (R_e) in series to a parallel circuit element that branches into, the double layer capacitance (C_{dl}) and the resistance to charge transfer (R_{ct}). The calculated values from using this model circuit are displayed in Table 1. The C_{dl} and the R_e change minimally over the 100 cycles. However, the R_{ct} more than doubles from the fresh cell to the 100th cycle. This is taken to mean the interface layer is gradually increasing in resistance, which is believed to be the result of incomplete dissolution of the interface upon reversal of the current's polarity leading to an SEI of constantly increasing thickness. This is corroborated by the increasing plateau voltage and the compounding of imperfect Coloumbic efficiency. Given the constant nature of R_e relative to R_{ct} the bulk electrolyte remains largely unaffected by the current decay that is occurring at the electrode–electrolyte interface. Lastly the long term cycling stability of the hybrid electrolyte system confirms suppression of dendrite growth. Although the interface needs to be slightly modified so that it reaches a steady state; the ability to deploy batteries containing metallic lithium would result in a large boost in capacity.

4. Conclusions

Polymer electrolyte systems present a unique opportunity for the future of lithium batteries. The solid sulfur based IL hybrid

electrolyte system developed maintains many of the pure polymer systems ideal properties while improving its low temperature conductivity over previously investigated IL chemistries. Our casting procedure yields homogenous freestanding films that would ultimately be able to withstand many of the processing steps for a commercial battery system. The hybrid electrolyte has demonstrated sufficient ionic conductivity (0.117 mS cm^{-1}) at 0 °C, and 1.20 mS cm^{-1} at 25 °C. At the temperature of the human body, ionic conductivity of the hybrid electrolyte system approaches 10 mS cm^{-1}, ultimately boding well for the development of a safer battery for biological purposes. The hybrid electrolyte demonstrated progress towards an electrolyte that will work for higher voltage and higher capacity lithium battery systems. The system possesses reversible cathodic stability exceeding 4.5 V and long term cycling stability against metallic lithium.

Acknowledgements

This work was supported by NSF grant no. CBET-0728975 and the generous donation of John and Maureen Hendricks. NMR work was performed at the University of Maryland Analytical NMR Service & Research Center, MS work was performed at University of Maryland Mass Spectrometry Facility and the Raman spectroscopy was performed at the University of Maryland Surface Analysis Center. Special thanks to Dr. Ayan Ghosh and Dr. Chunsheng Wang for productive discussions on batteries and electrolytes.

References

[1] K. Xu, Chem. Rev. 104 (2004) 4303–4417.
[2] M. Armand, Faraday Discuss. Chem. Soc. (1989) 65–76.
[3] F.M. Gray, Solid Polymer Electrolytes, VCH Publishers, New York, 1991.
[4] J.R. MacCallum, M.J. Smith, C.A. Vincent, Solid State Ionics 11 (1984) 307.
[5] T. Tatsuma, M. Taguchi, M. Iwaku, T. Sotomura, N. Oyama, J. Electroanal. Chem. 472 (1999) 142–146.
[6] A. Ghosh, P. Kofinas, J. Electrochem. Soc. 155 (2008) A428–A431.
[7] T. Uno, S. Kawaguchi, M. Kubo, T. Itoh, J. Power Sources 178 (2008) 716–722.
[8] H. Pitawala, M. Dissanayake, V. Seneviratne, B.E. Mellander, I. Albinson, J. Solid State Electrochem. 12 (2008) 783–789.
[9] Y.W. Chen-Yang, Y.L. Wang, Y.T. Chen, Y.K. Li, H.C. Chen, H.Y. Chiu, J. Power Sources 182 (2008) 340–348.
[10] A.M. Stephan, K.S. Nahm, Polymer 47 (2006) 5952–5964.
[11] J.H. Shin, W.A. Henderson, S. Passerini, J. Electrochem. Soc. 152 (2005) A978–A983.
[12] J.H. Shin, W.A. Henderson, S. Passerini, Electrochem. Solid State 8 (2005) A125–A127.
[13] J.H. Shin, W.A. Henderson, S. Passerini, Electrochem. Commun. 5 (2003) 1016–1020.
[14] B. Garcia, S. Lavallée, G. Perron, C. Michot, M. Armand, Electrochim. Acta 49 (2004) 4583–4588.
[15] S.-K. Chariclea, T.C. Richard, J. Electrochem. Soc. 141 (1994) 873–875.
[16] H. Nakagawa, S. Izuchi, K. Kuwana, T. Nukuda, Y. Aihara, J. Electrochem. Soc. 150 (2003) A695–A700.
[17] E. Paillard, Q. Zhou, W.A. Henderson, G.B. Appetecchi, M. Montanino, S. Passerini, J. Electrochem. Soc. 156 (2009) A891–A895.
[18] J.B. Goodenough, Y. Kim, Chem. Mater. 22 (2009) 587–603.
[19] H. Cheng, C. Zhu, B. Huang, M. Lu, Y. Yang, Electrochim. Acta 52 (2007) 5789–5794.
[20] J. Sun, D.R. MacFarlane, M. Forsyth, Solid State Ionics 147 (2002) 333–339.
[21] P.E. Stallworth, J.J. Fontanella, M.C. Wintersgill, C.D. Scheidler, J.J. Immel, S.G. Greenbaum, A.S. Gozdz, J. Power Sources 81–82 (1999) 739–747.
[22] J.M. Tarascon, M. Armand, Nature 414 (2001) 359–367.
[23] H. Matsumoto, T. Matsuda, Y. Miyazaki, Chem. Lett. 29 (2000) 1430–1431.
[24] K. Tsunashima, M. Sugiya, Electrochem. Commun. 9 (2007) 2353–2358.
[25] S. Fang, L. Yang, C. Wei, C. Peng, K. Tachibana, K. Kamijima, Electrochem. Commun. 9 (2007) 2696–2702.
[26] W.H. Meyer, Adv. Mater. 10 (1998) 439–448.
[27] L.J. Krause, W. Lamanna, J. Summerfield, M. Engle, G. Korba, R. Loch, R. Atanasoski, J. Power Sources 68 (1997) 320–325.